Supporting Information for

A Near-Infrared Emitting Covalent Organic Framework with AIE Characteristic for Light-Emitting Diodes

Jingrui Liu, [a] *Xilang Jin,* [*a] *Xiao Li,* [a] *Xuehao Ma,* [a] *Peiyu Cui,* [b] *Tongyu Zhang,* [c] *Wenxing Chen,* [a] *Wenhuan Huang**[b]

[a] School of Materials and Chemical Engineering, Xi'an Technological University, Xi'an 710021, PR China.
[b] Key Laboratory of Chemical Additives for China National Light Industry, College of Chemistry and Chemical Engineering, Shaanxi University of Science and Technology, Xi'an 710021, China.
[c] College of Materials Science and Engineering, Sichuan University, Chengdu 610064, China.

Contents

1. Experimental Section

1.1 Materials

m-Tolidine (MT) and 1,3,5-benzenetricarboxaldehyde (BTA) were purchased from Sain Chemical Technology (Shanghai) Co., Ltd.

2-hydroxy-1,3,5-benzenetrialdehyde (HBTA) was purchased from Shanghai McLean Biochemical Technology Co., Ltd.

In this experiment, all reagents, including tetrahydrofuran (THF), 1,4-dioxane, acetone, and toluene, were directly procured and used without the need for further purification.

1.2 Instrument

X-ray diffraction (XRD) spectra were determined using a Bruker D_2 PHASER X-ray diffractometer. Fourier-transform infrared spectra (FT-IR) were recorded with an IS50 Fourier Infrared Spectrometer. X-ray photoelectron spectroscopy (XPS) was gathered using a Thermo Scientific K-Alpha instrument. Nitrogen adsorption-desorption isotherms were measured with a BELSORP MAX II nitrogen adsorption-desorption specific surface area analyzer. Thermal stability was assessed via a TGA/DSC1 synchronous thermal analyzer. Material morphology was observed using a Quanta FEG400 scanning electron microscope (SEM). Fluorescence performance experiments were conducted with a Quanta Master8000 steady-state transient fluorescence spectrometer.

1.3 Synthesis of MT-BTA-COF

m-Tolidine (MT) (64 mg, 0.30 mmol) and 1,3,5-Benzenetricarboxaldehyde (BTA) (32 mg, 0.20 mmol) were added to a 15 mL Pyrex tube. Then, mix thoroughly using ultrasonic agitation, and add solvent, and toluene (3 mL). Next, introduce the acetic acid solution (6M, 0.3 mL). Seal the Pyrex tube after three vacuum pulls and nitrogen gas cycles, and place it in an oven at 120 ℃ for 72 hours. After cooling to room temperature, separate the solid powder using a Buchner funnel and wash successively with 1,4-Dioxane, tetrahydrofuran (THF), and acetone. Finally, dry in a vacuum oven at 60 ℃ for 12 hours to yield 84.3 mg of powder, with an approximate yield of 88%.

1.4 Synthesis of MT-HBTA-COF

In a 15 ml Pyrex tube, the addition of m-Tolidine (MT) (64 mg, 0.30 mmol) and 2-hydroxy-1,3,5-benzotriazole (HBTA) (36 mg, 0.20 mmol) were added. Add 3 mL of the solvent, toluene, and mix uniformly using ultrasound. Then, introduce the acetic acid solution (6M, 0.3 mL). Seal the Pyrex tube through three cycles of vacuum and nitrogen gas purging, and place it in an oven set at 120 ℃ for 72 hours. After cooling to room temperature, use a Buchner funnel to filter and isolate the solid powder. Wash successively with dioxane, THF, and acetone. Dry in a vacuum oven at 60 ℃ for 12 hours to obtain 89.35 mg of powder, yielding approximately 90%.

2.XRD

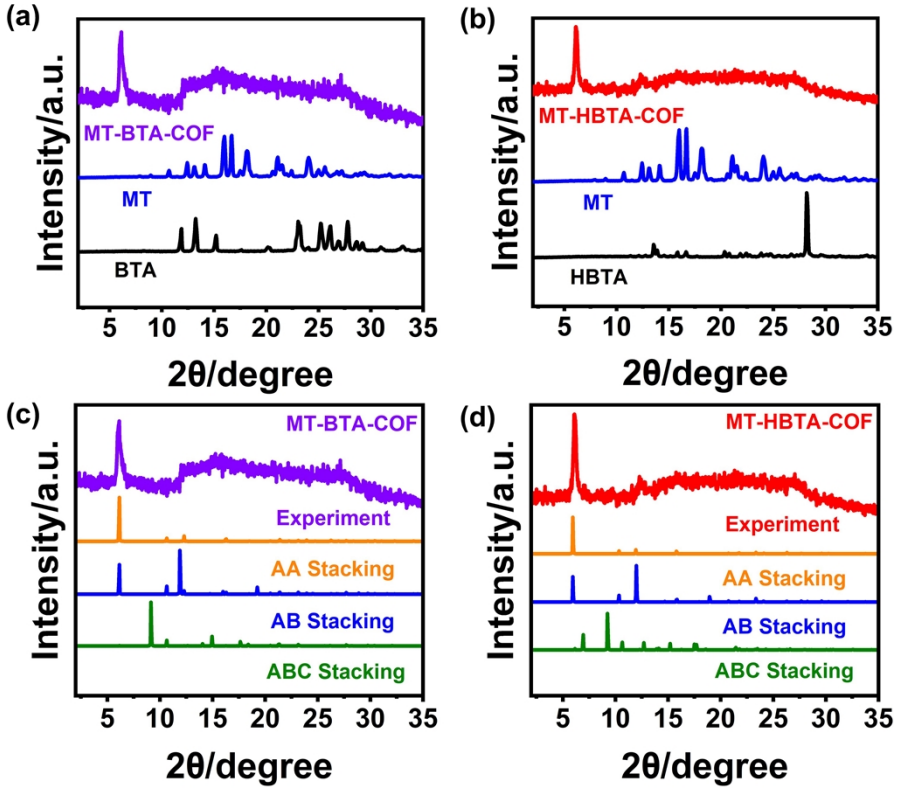

Figure S1. (a) XRD spectra of MT-BTA-COF and its precursors; (b) XRD spectra of MT-HBTA-COF and its precursors. XRD spectra of the AA stacking, AB stacking, and ABC stacking crystal structures of (c) MT-BTA-COF and (d) MT-HBTA-COF compared with experimental XRD spectra.

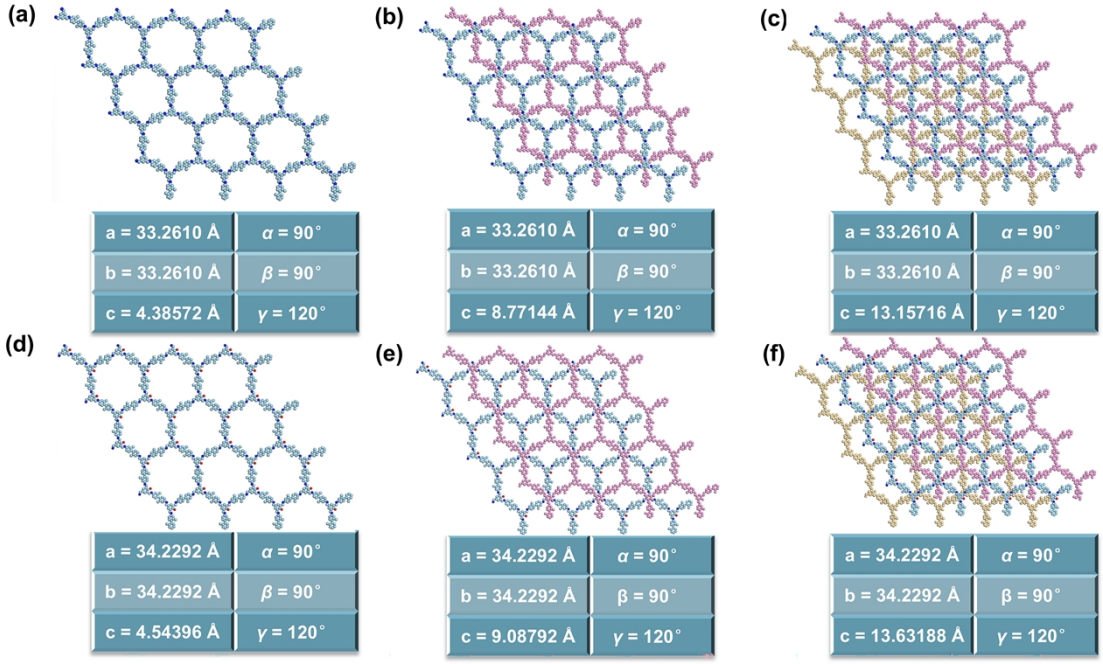

Figure S2. Schematic diagrams of crystal structures and cell parameters for simulated (a) AA stacking, (b) AB stacking, and (c) ABC stacking of MT-BTA-COF; and for simulated (d) AA stacking, (e) AB stacking, and (f) ABC stacking of MT-HBTA-COF.

3. SEM images

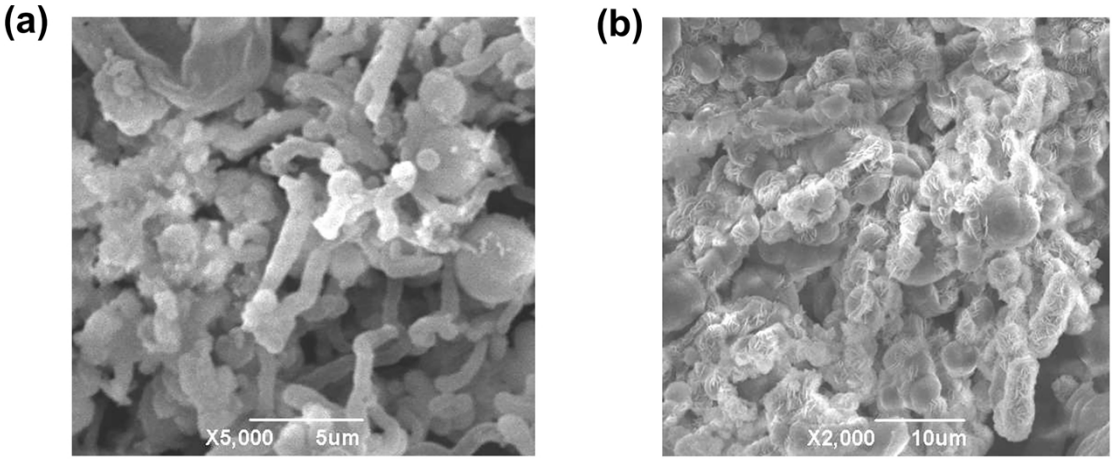

Figure S3. SEM images of (a) MT-BTA-COF and (b) MT-HBTA-COF.

4. N_2 Adsorption-Desorption Testing

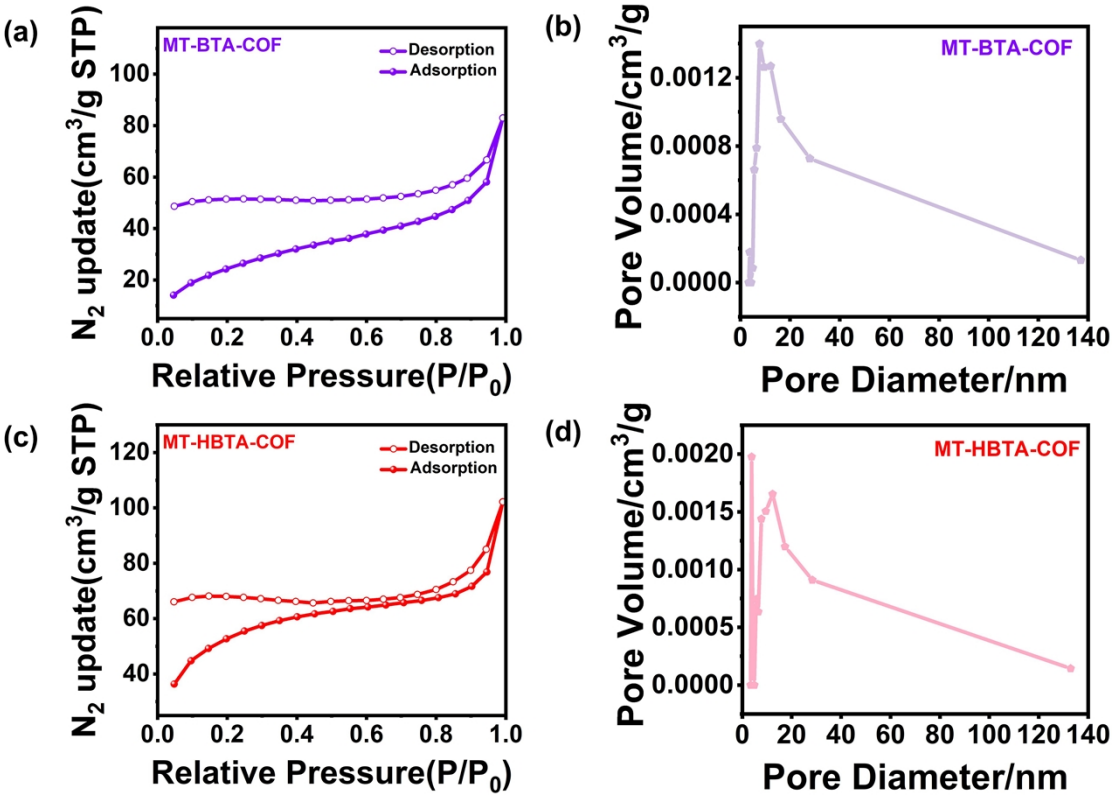

Figure S4. (a) Nitrogen adsorption-desorption isotherms of MT-BTA-COF; (b) Pore size distribution curves for MT-BTA-COF; (c) Nitrogen adsorption-desorption isotherms of MT-HBTA-COF; (d) Pore size distribution curves for MT-HBTA-COF.

5. FT-IR

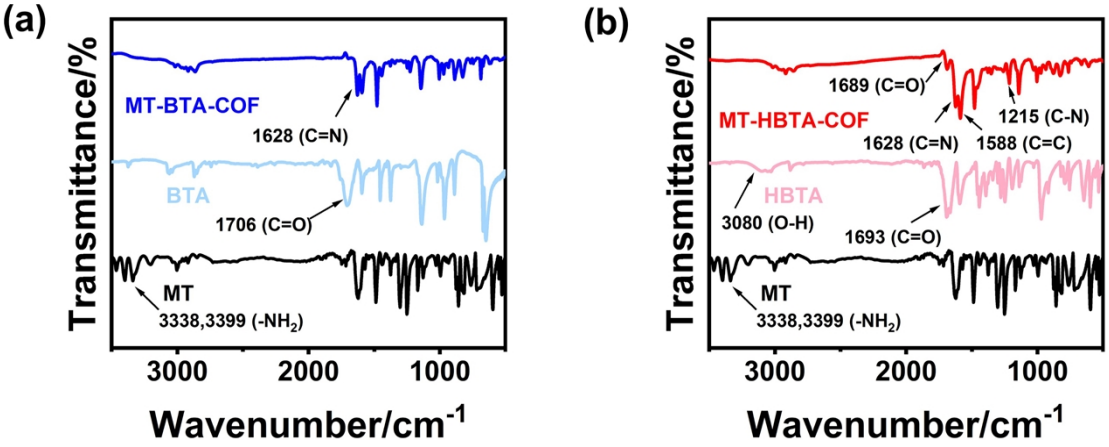

Figure S5. FT-IR spectra of (a) MT-BTA-COF and (b) MT-HBTA-COF with their respective raw materials.

FT-IR spectra confirmed the formation of imine linkages in MT-BTA-COF and MT-BTA-COF, as evidenced by the appearance of characteristic C=N stretching vibration peaks at 1628 cm^{-1} and the disappearance of the stretching vibrational peak of the $-NH_2$ group of the feedstock MT at 3200-3400 cm^{-1}. At the same time, the emergence of the characteristic C-N stretching peak at 1215 cm^{-1} and the formation of the C=O vibrational stretching signal at 1689 cm^{-1} in MT-HBTA-COF indicate the formation of keto-enol tautomerism between the aldehyde and amine groups of the building unit.

Compared with HBTA monomer, the intensity of the -OH stretching peak at 3100-3000 cm^{-1} in MT-HBTA-COF is weakened due to the formation of ketoamine structure, and the peak is red-shifted after the formation of hydrogen bonding, which may be overlapped with the C-H bonding at 3000-2900 cm^{-1}.

6. XPS spectra

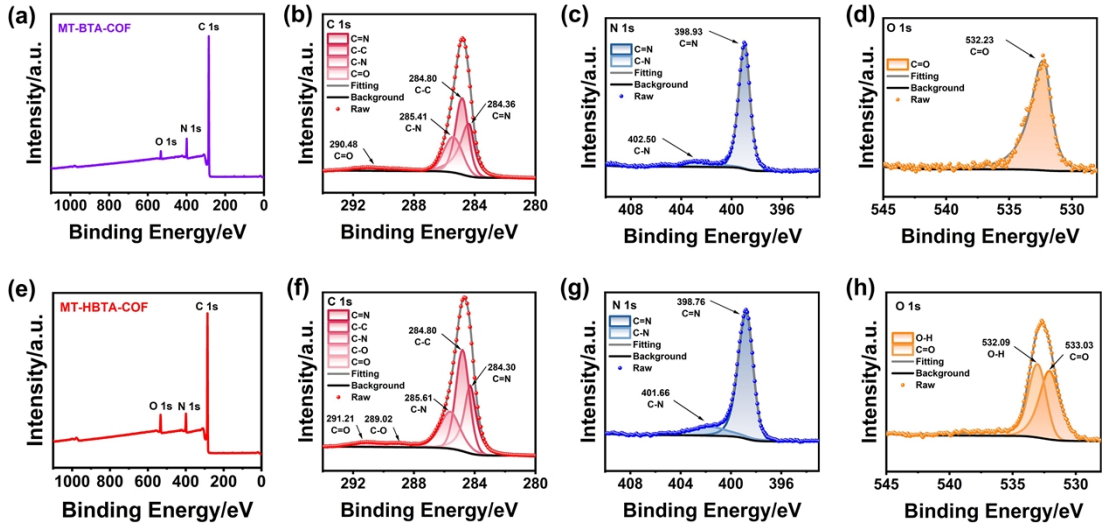

Figure S6. (a) XPS spectra of MT-BTA-COF; (b) Comparison of C 1s XPS spectra between MT-HBTA-COF and its precursors; (c) N 1s XPS spectrum of MT-BTA-COF; (d) O 1s XPS spectrum of MT-BTA-COF; (e) XPS spectra of MT-HBTA-COF; (f) C 1s XPS spectrum of MT-HBTA-COF; (g) N 1s XPS spectrum of MT-HBTA-COF; (h) O 1s XPS spectrum of MT-HBTA-COF.

7. ^{13}C NMR

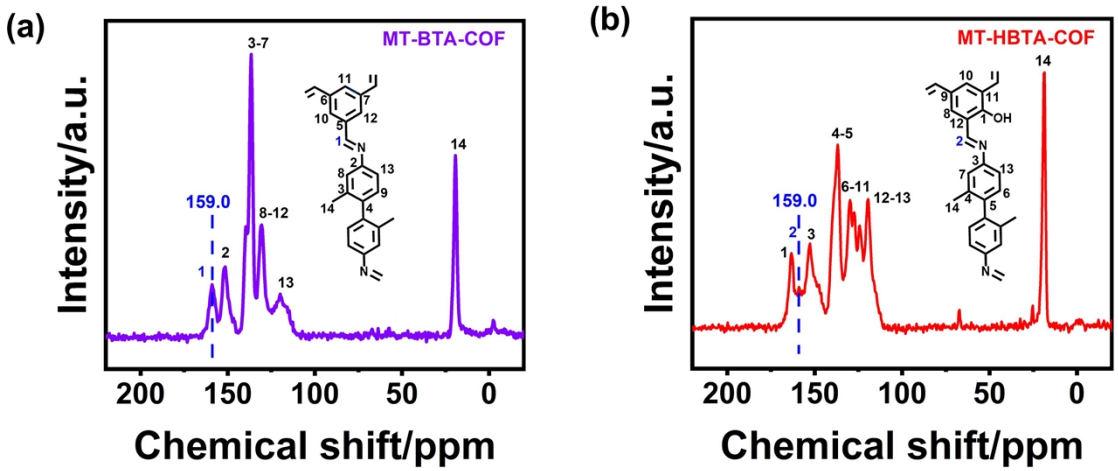

Figure S7. ^{13}NMR spectra of (a) MT-BTA-COF and (b) MT-HBTA-COF.

8. Fluorescence properties

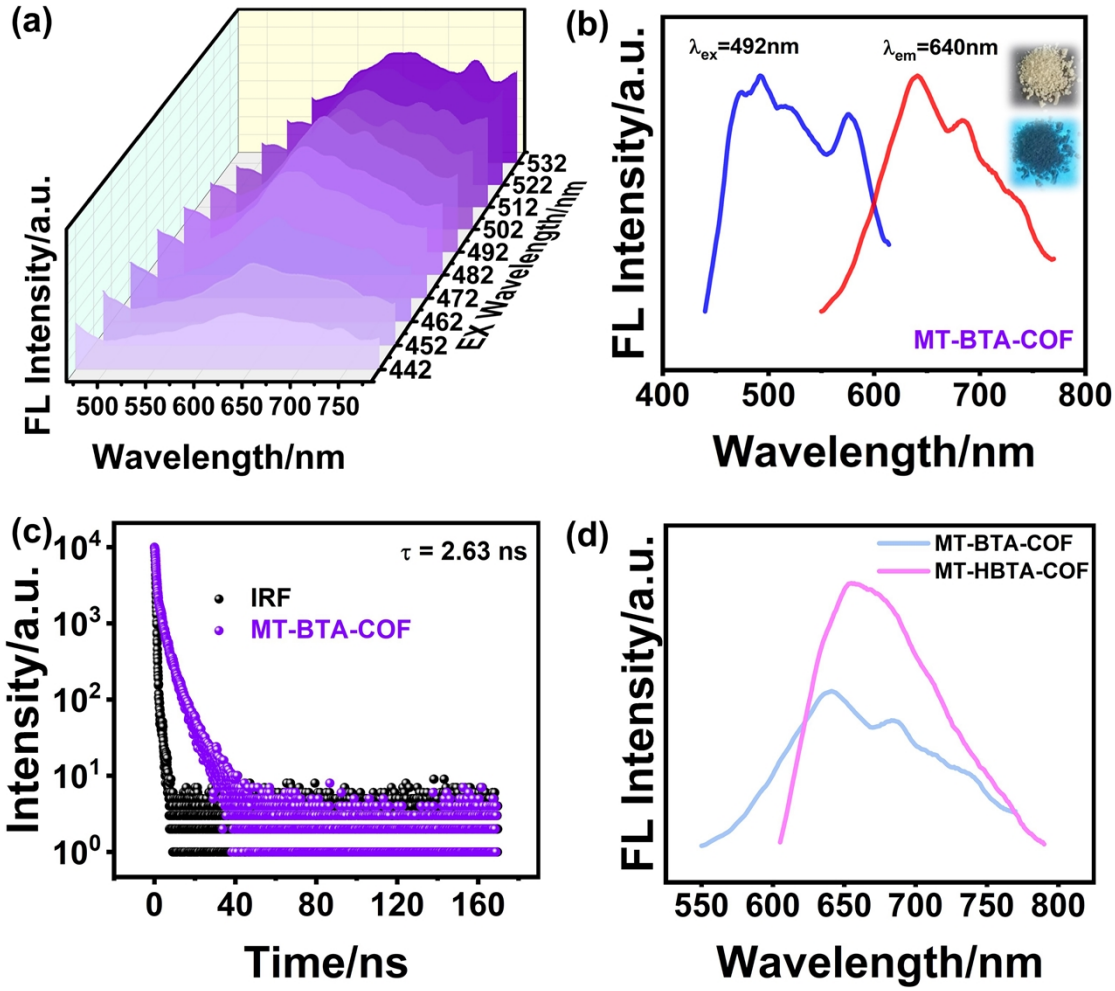

Figure S8. (a)Fluorescence spectra of solid-state MT-BTA-COF under different excitation wavelengths; (b)Fluorescence excitation-emission spectra of solid-state MT-BTA-COF; (the insert shows photographs of solid-state powder MT-BTA-COF under natural light and a 365 nm UV lamp) (c) Fluorescence decay curve with IRF of solid-state powder MT-BTA-COF; (d) Comparative fluorescence spectra of solid powders MT-BTA-COF and MT-HBTA-COF.

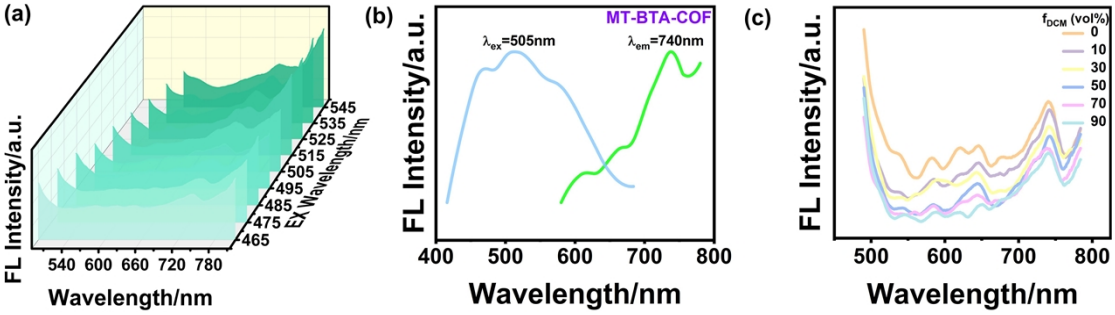

Figure S9. (a) Fluorescence spectra of MT-BTA-COF suspensions dispersed in tetrahydrofuran at different excitation wavelengths; (b) Fluorescence excitation-emission spectra of MT-BTA-COF suspensions dispersed in tetrahydrofuran; (c) fluorescence spectra of MT-BTA-COF in different ratios of DCM/THF mixed solvents.

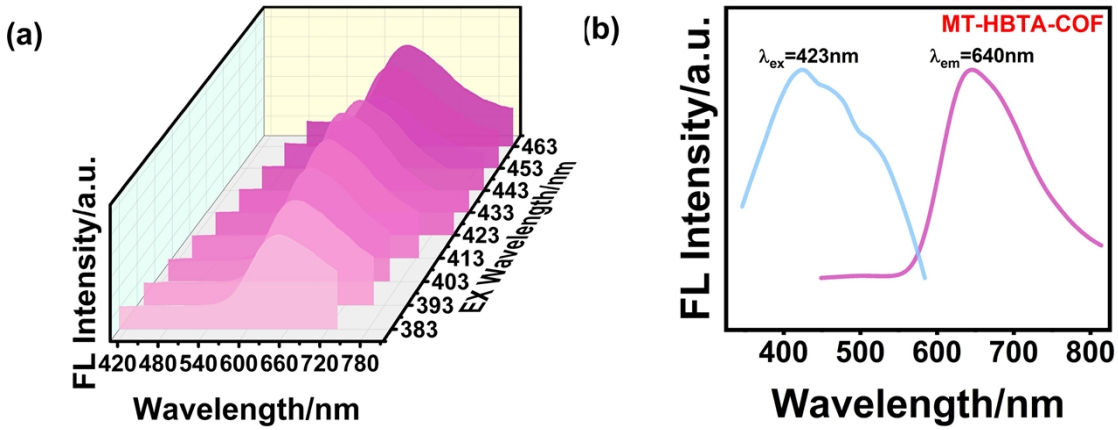

Figure S10. (a) Fluorescence spectra of MT-HBTA-COF suspensions dispersed in tetrahydrofuran at different excitation wavelengths; (b) Fluorescence excitation-emission spectra of MT-HBTA-COF suspensions dispersed in tetrahydrofuran.

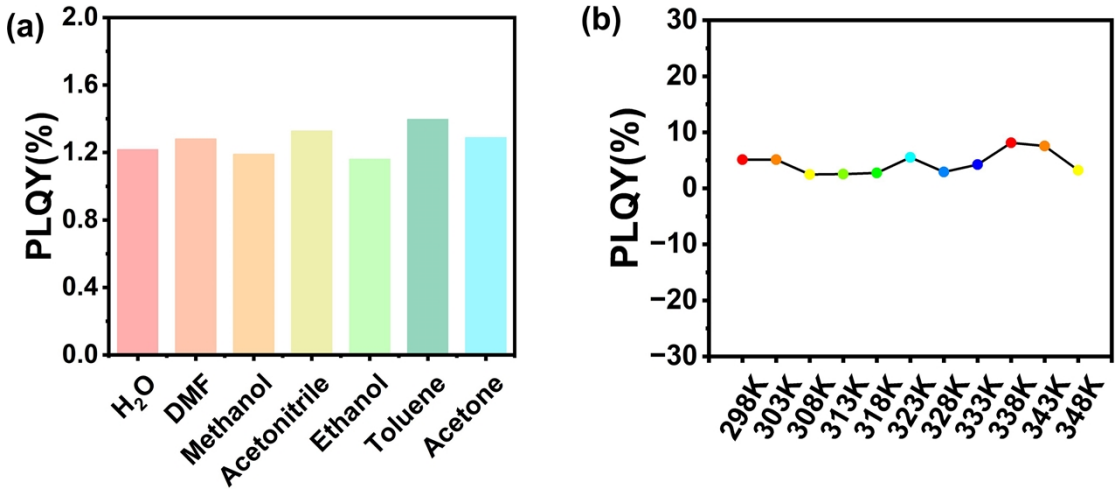

Figure S11 (a) PLQY of MT-HBTA-COF in different solvents; (b) Solid state PLQY of MT-HBTA-COF at different temperatures.

The liquid-state quantum yields of MT-HBTA-COF in various solvents, including H2O, N,N-dimethylformamide (DMF), methanol, acetonitrile, ethanol, toluene, acetone, tetrahydrofuran, and dichloromethane, were measured at 1.22%, 1.28%, 1.19%, 1.33%, 1.16%, 1.40%, and 1.29%, respectively. In solid-state conditions at temperatures of 298K, 303K, 308K, 313K, 318K, 323K, 328K, 333K, 338K, 343K, and 348K, the quantum yields were recorded as 5.13%, 5.12%, 2.46%, 2.54%, 2.73%, 5.53%, 2.91%, 4.22%, 8.12%, 7.55%, and 3.22%, respectively.

9. LED

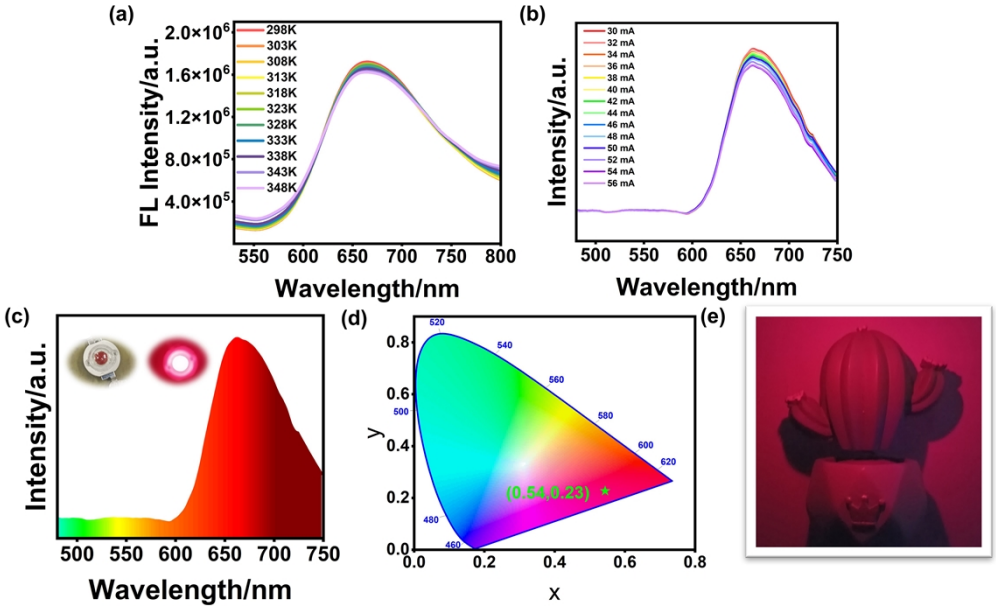

Figure S12. (a) PL emission spectra of MT-HBTA-COF at different temperatures (λex = 469 nm); (b) The emission spectrum of red LED made of MT-HBTA-COF as down-conversion luminescent material under different working current; (c) The emission spectrum of red LED made of MT-HBTA-COF as down-conversion luminescent material (inset is the contrast photo of LED in non-working state and working state); (d) CIE chroma coordinate of the corresponding LED;(e) Corresponding LED working image.

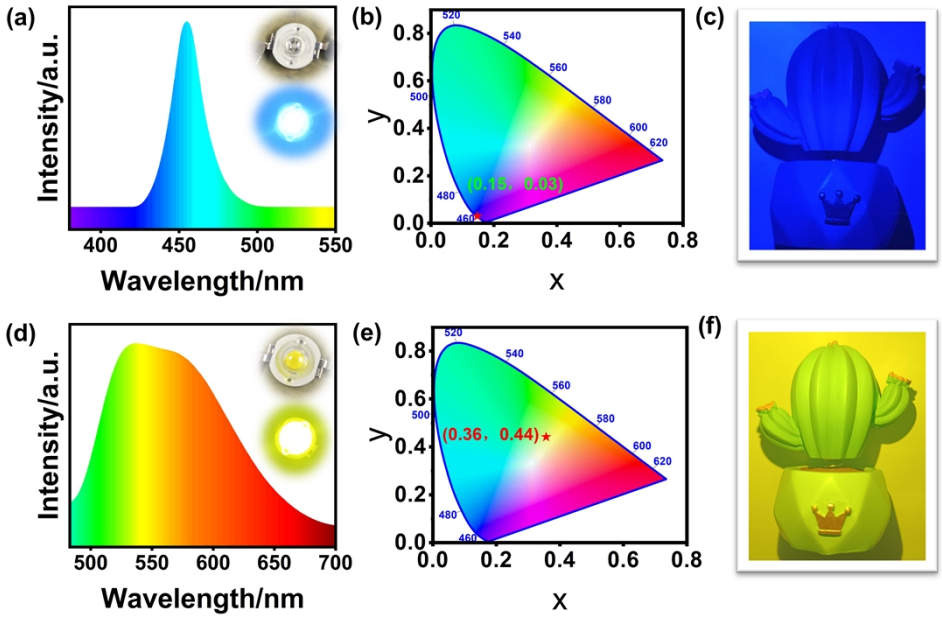

Figure S13. (a) The emission spectrum of blue chip (inset is the contrast photo of blue chip in non-working state and working state) ;(b) CIE chroma coordinate of the corresponding blue chip;(c) Corresponding blue chip working image. (d) The emission spectrum of yellow LED made of yellow phosphor as down-conversion luminescent material (inset is the contrast photo of LED in non-working state and working state) ;(e) CIE chroma coordinate of the corresponding LED;(f) Corresponding LED working image.

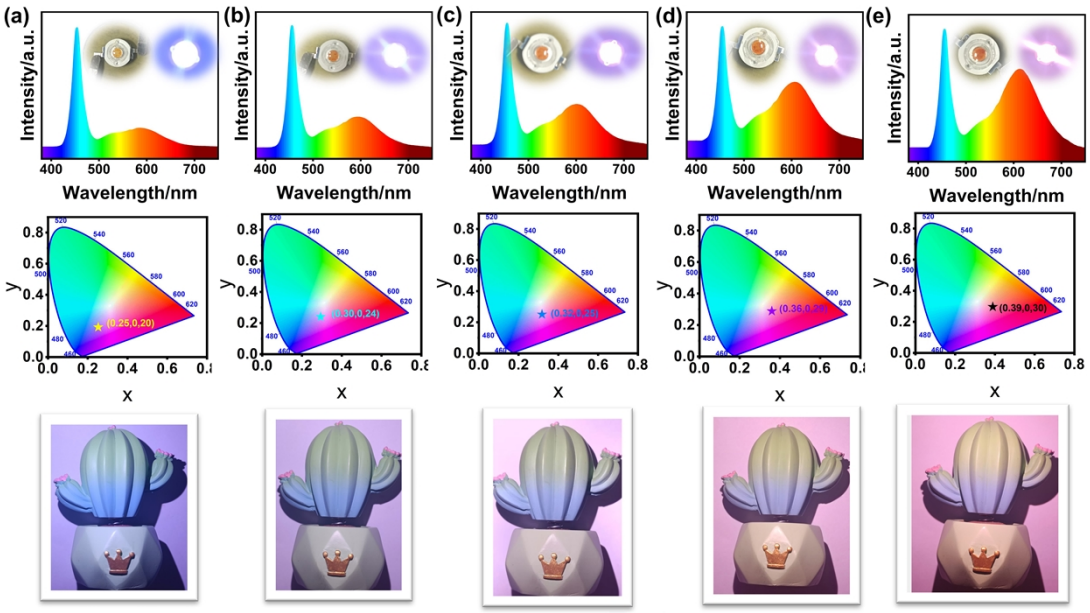

Figure S14. Characterization of white light LEDs. When the concentrations of phosphor and MT-HBTA-COF mixture in A-B adhesive are (a) 0.5, (b) 1.0, (c) 1.5, (d) 2.0, and (e) 2.5 wt%, respectively, the emission spectrum of white LED (inset is the contrast photo of LED in non-working state and working state), CIE chroma coordinate of the corresponding LED and corresponding LED working image.

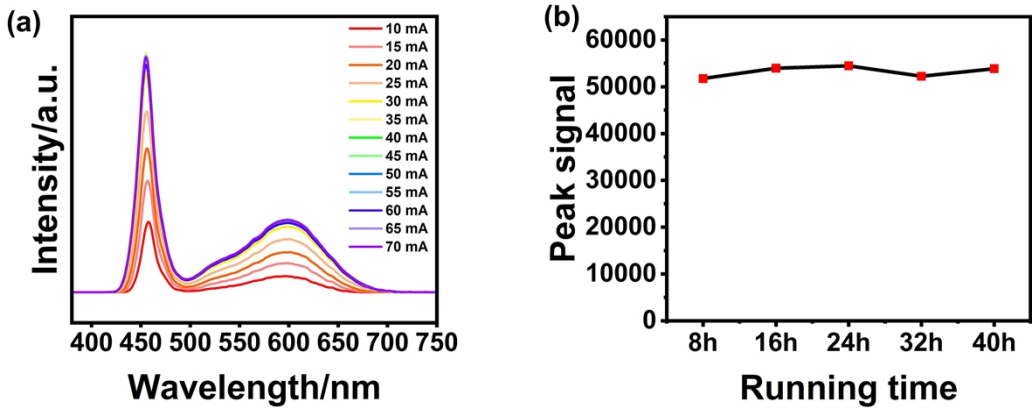

Figure S15. (a) The emission spectrum of No.3 white LED under different working current ;(b) Linear relationship between No.3 LED peak signal and running time.

10. Fractional Atomic Coordinates for the Unit Cell

Table S1. Atomic coordinates of the MT-BTA-COF model refined by Pawley.

Atom	x	y	z
C1	-1.148	10.858	-2.271
C2	-1.058	10.068	-2.069
C3	-0.356	9.715	-2.362
C4	0.286	10.139	-2.834
C5	0.183	10.934	-3.107
C6	-0.532	11.28	-2.815
C7	1.065	9.762	-2.806
C8	1.657	10.111	-2.043
C9	2.328	9.712	-1.701
C10	2.425	8.955	-2.104
C11	1.878	8.621	-2.97
C12	1.194	9.009	-3.31
N13	-1.822	11.26	-1.805
C14	0.808	11.44	-3.693
C15	0.616	8.578	-4.153
C16	-4.321	12.156	0.426
C17	-4.408	11.375	0.107
C18	-3.807	10.993	-0.556
C19	-3.123	11.379	-0.911
C20	-3.037	12.156	-0.581
C21	-3.629	12.548	0.094
C22	-3.501	13.363	0.436
C23	-5.114	10.932	0.441
C24	-2.495	10.946	-1.567
N25	3.042	8.522	-1.51
C26	4.293	7.794	-0.086
C27	3.644	7.393	-0.576
C28	3.558	6.612	-0.284
C29	4.102	6.231	0.513
C30	4.744	6.64	1.016
C31	4.85	7.42	0.703
C32	5.561	7.824	1.148
C33	3.033	7.782	-1.35
C34	3.994	5.402	0.766
C35	6.42	8.948	0.913
C36	7.047	8.682	1.673
C37	7.749	9.088	1.685
C38	7.85	9.763	0.933

C39	7.195	10.065	0.249
C40	6.493	9.649	0.248
C41	8.642	10.121	0.875
C42	8.748	10.883	1.313
C43	9.477	11.242	1.251
C44	10.12	10.851	0.757
C45	10.023	10.088	0.328
C46	9.302	9.714	0.402
N47	5.721	8.509	0.703
N48	10.846	11.259	0.609
C49	7.204	10.81	-0.509
C50	9.284	8.891	-0.064
C51	4.39	4.223	1.852
C52	3.708	3.796	1.633
C53	3.708	3	1.773
C54	4.386	2.606	2.144
C55	5.065	3.045	2.446
C56	5.051	3.847	2.309
C57	4.391	1.75	2.022
C58	4.947	1.422	1.174
C59	4.935	0.642	0.871
C60	4.363	0.158	1.42
C61	3.809	0.473	2.276
C62	3.809	1.262	2.579
N63	4.441	5.032	1.59
N64	4.297	-0.643	1.079
C65	5.822	2.701	2.894
C66	3.171	1.548	3.469

Table S2. Atomic coordinates of the MT-HBTA-COF model refined by Pawley.

Atom	x	y	z
C1	-1.568	11.569	-2.274
C2	-1.555	10.807	-1.893
C3	-0.881	10.382	-2.182
C4	-0.191	10.702	-2.832
C5	-0.212	11.473	-3.249
C6	-0.903	11.891	-2.966
C7	0.563	10.25	-2.872
C8	1.283	10.568	-2.302
C9	1.959	10.132	-2.075
C10	1.939	9.367	-2.409
C11	1.252	9.053	-3.071
C12	0.561	9.478	-3.288
N13	-2.208	12.048	-1.866
C14	0.475	11.883	-3.976
C15	-0.154	9.068	-3.942
C16	-4.747	13.233	0.117
C17	-4.95	12.491	-0.274
C18	-4.35	12.051	-0.839
C19	-3.545	12.339	-0.997
C20	-3.336	13.087	-0.571
C21	-3.95	13.542	-0.039
C22	-3.787	14.353	0.267
C23	-5.796	12.193	-0.111
C24	-2.94	11.817	-1.53
N25	2.611	8.922	-2.01
C26	4.037	8.165	-1.105
C27	3.279	7.79	-1.313
C28	3.184	7.019	-1.007
C29	3.823	6.625	-0.438
C30	4.581	7.009	-0.192
C31	4.694	7.777	-0.575
C32	5.511	8.155	-0.517
C33	2.572	8.193	-1.824
C34	3.677	5.813	-0.123
C35	6.383	9.282	-0.371
C36	7.064	9.01	-1.031
C37	7.82	9.389	-0.911
C38	7.925	10.043	-0.12
C39	7.222	10.342	0.492
C40	6.462	9.956	0.35
C41	8.759	10.417	-0.05

C42	8.86	11.183	-0.428
C43	9.632	11.541	-0.492
C44	10.326	11.141	-0.182
C45	10.238	10.382	0.183
C46	9.468	10.012	0.266
N47	5.603	8.886	-0.419
N48	11.132	11.479	-0.285
C49	7.238	11.06	1.297
C50	9.454	9.197	0.711
C51	4.086	4.684	1.09
C52	3.46	4.18	0.658
C53	3.494	3.409	0.934
C54	4.149	3.114	1.645
C55	4.767	3.632	2.13
C56	4.718	4.408	1.856
C57	4.211	2.271	1.701
C58	4.922	1.952	1.202
C59	4.966	1.172	1.009
C60	4.297	0.687	1.318
C61	3.609	0.989	1.893
C62	3.548	1.771	2.077
N63	4.129	5.471	0.735
N64	4.27	-0.108	1.021
C65	5.498	3.397	2.907
C66	2.76	2.027	2.66
O67	-2.523	13.358	-0.642
O68	5.212	6.621	0.415

Table S3. The element content of MT-BTA-COF and MT-HBTA-COF.

Sample		C (%)	H (%)	N (%)	O (%)
MT-BTA-COF	Found	81.54	6.36	9.01	
	Calculated	82.02	6.02	11.96	
MT-HBTA-COF	Found	79.05	6.56	8.64	5.24
	Calculated	78.45	5.76	11.44	4.35

11. Performance data of the LEDs

Table S4. The performance data of blue chip and LED using yellow phosphor or MT-HBTA-COF as down-conversion material.

Test subject	Luminous efficiency ($lm \cdot w^{-1}$)	Ra	CCT (K)	CIE (x, y)
Blue chip	21.23	69.5	100000	(0.15,0.03)
yellow phosphor	18.45	61.5	4785	(0.36,0.44)
MT-HBTA-COF	0.02	16.1	1001	(0.54,0.23)

Table S5. The performance data of LED using MT-HBTA-COF as down-conversion material under different working current.

Working Current	Luminous Efficiency ($lm \cdot w^{-1}$)	Ra	CCT (K)	CIE (x, y)
30 mA	0.02	25.5	1001	(0.57,0.24)
32 mA	0.02	20.8	1001	(0.56,0.23)
34 mA	0.02	23.8	1001	(0.56,0.23)
36 mA	0.02	25.2	1001	(0.57,0.23)
38 mA	0.02	18.1	1001	(0.55,0.23)
40 mA	0.02	24.7	1001	(0.57,0.24)
42 mA	0.02	18.9	1001	(0.57,0.23)
44 mA	0.02	20.8	1001	(0.56,0.23)
46 mA	0.02	19.1	1001	(0.56,0.23)
48 mA	0.02	19.3	1001	(0.55,0.22)
50 mA	0.02	16.1	1001	(0.54,0.23)
52 mA	0.02	15.2	1001	(0.54,0.22)
54 mA	0.02	19.8	1001	(0.55,0.23)
56 mA	0.02	16.9	1001	(0.55,0.23)

Table S6. The performance data of LED using mixtures of phosphor and MT-HBTA-COF as down-conversion material.

No. of LEDs	Quality ratio (yellow phosphor and MT-HBTA-COF)	Concentration of the mixtures (wt.%)	Luminous efficiency ($lm \cdot w^{-1}$)	Ra	CCT (K)	CIE (x, y)
1	3:1	0.5	56.15	72.7	100000	(0.25,0,20)
2	3:1	1.0	41.8	75.5	11500	(0.30,0,24)
3	3:1	1.5	38.25	77.1	7281	(0.32,0,25)
4	3:1	2.0	33.01	80.8	3732	(0.36,0,29)
5	3:1	2.5	24.13	75.1	2826	(0.39,0,30)

Table S7. The performance data of No.3 LED using mixtures of phosphor and MT-HBTA-COF as

down-conversion material under different working current.

Working Current	Luminous efficiency ($lm \cdot w^{-1}$)	Ra	CCT (K)	CIE (x, y)
10 mA	15.53	60.2	13138	(0.32,0.22)
15 mA	20.49	67.6	8890	(0.31,0.24)
20 mA	24.95	71.3	7919	(0.32,0.24)
25 mA	30.29	73.9	7472	(0.32,0.25)
30 mA	35.38	75.1	7335	(0.32,0.25)
35 mA	38.44	75.9	7336	(0.32,0.25)
40 mA	38.4	75.7	7323	(0.32,0.25)
45 mA	38.25	76	7284	(0.32,0.25)
50 mA	38.25	77.1	7281	(0.32,0.25)
55 mA	38.43	76.3	7185	(0.32,0.25)
60 mA	37.03	76.1	7237	(0.32,0.25)
65 mA	37.26	76.3	7234	(0.32,0.25)
70 mA	37.48	76.1	7228	(0.32,0.25)

Table S8. The performance data of commercial WLED.

Test subject	Luminous efficiency ($lm \cdot w^{-1}$)	Ra	CCT (K)	CIE (x, y)
The standard WLED	160.48	64.7	6312	(0.32,0.33)

Table S9 Other reported examples of phosphors used for LED.

No.	Chemical formula	synthetic method	Excitation wavelength	Emission wavelength	WLED-CIE coordinates	WLED-CCT (K)	Ref.
1	$Gd_{3-y}Ca_{y-0.02}GaO_6$:0.02Eu^{2+} (y=0.2)	1500°C High temperature solid-state method	460 nm	650 nm	(0.38, 0.39)	3999	1
2	$BaLa_{0.93}MgNbO_6$: 0.05Sm^{3+},0.02Y^{3+}	1400°C High temperature solid-state method	Max: 406 nm	Max: 599 nm	(0.35, 0.34)	4938	2
3	Ca_2GaNbO_6: 0.03Sm^{3+}	1450°C High temperature solid-state method	Max: 406 nm	Max: 599 nm	No data	3877	3
4	$BaLaGaO_4$: 0.30Eu^{3+}	1300°C High temperature solid-state method	Max: 394 nm	Max: 703 nm	(0.32, 0.34)	6024	4
5	$n_{3\%}$-$SrLaScO_4$:4%Eu	600°C, 1400°C, 1500°C employ $(NH_4)_2SO_4$-assisted sintering	450 nm	620 nm	(0.38, 0.37)	4005	5

6	R-CDs	180℃ solvothermal method	385 nm	Max: 600 nm	(0.41, 0.38)	3248	6
7	AIE CD1	microwave heating method	470 nm	550 nm	(0.32, 0.42) (0.29, 0.38)	No data	7
8	AIE Hz-$COF_{TFBE-ODH}$	120 ℃ solvothermal method	397 nm	546 nm	(0.34, 0.35)	No data	8
9	AIE HOF-76⊃DSMI	No data	460 nm	508 nm	(0.33, 0.33)	5490	9
10	AIE COF	110 ℃ Hot reflux method	499 nm	590 nm	(0.42, 0.42)	3348	10
11	This work (MT-HBTA-COF)	120 ℃ solvothermal method	469 nm	657 nm	(0.32, 0.25)	7281	This work

1. X. Huo, Z. Wang, X. Meng, J. Zhang, Y. Wang and P. Li, *Journal of Materials Chemistry C*, 2024, **12**, 4287-4295.
2. Y. Huo, R. Chen, Y. Yang, L. Zhou, M. Chang, C. Li, W. Yang, H. Lin, L. Liu, S. Li and F. Zeng, *Ceramics International*, 2024, **50**, 48474-48484.
3. Y. Zhang, X. Guo, M. Zhang, R. Cui, J. Zhang and C. Deng, *Journal of Alloys and Compounds*, 2024, **1002**, 175459.
4. P. Ling-Hu, X. Guo, J. Hu, C. Deng and R. Cui, *Advanced Optical Materials*, 2023, **12**, 2301760.
5. Z. Yang, G. Liu, Y. Zhao, Y. Zhou, J. Qiao, M. S. Molokeev, H. C. Swart and Z. Xia, *Advanced Optical Materials*, 2022, **10**, 2102373.
6. Q. Han, W. Xu, J. Deng, X. Zhang, J. Li and Z. Peng, *ACS Applied Nano Materials*, 2023, **6**, 16373-16382.
7. Y. Zhang, P. Zhuo, H. Yin, Y. Fan, J. Zhang, X. Liu and Z. Chen, *ACS Appl Mater Interfaces*, 2019, **11**, 24395-24403.
8. H. Wan, X. Wang, Q. Nie, X. Wang, L. Wang and Y. Song, *Advanced Optical Materials***,** 2025, 2402907.
9. Y.-X. Lin, J.-X. Wang, C.-C. Liang, C. Jiang, B. Li and G. Qian, *RSC Advances*, 2022, **12**, 23411-23415.
10. X. Li, H. Tang, L. Gao, Z. Chen, H. Li, Y. Wang, K. Yang, S. Lu, K. Wang, Q. Zhou and Z. Wang, *Polymer*, 2022, **241**, 124474.